Investigation of the valence electronic states of Ti(IV) in Ti silicalite-1coupling X-ray emission spectroscopy and density functional calculations

Investigation of the valence electronic states of Ti(IV) in Ti silicalite-1 coupling X-ray emission spectroscopy and density functional calculations

Erik Gallo, Carlo Lamberti, Pieter Glatzel

Phys. Chem. Chem. Phys., 2011, 13, 19409–19419

doi: 10.1039/c1cp21556f

Investigation of the valence electronic states of Ti(IV) in Ti silicalite-1 coupling X-ray emission spectroscopy and density functional calculations

Erik Gallo, [1,2,3] Carlo Lamberti,[2,3] Pieter Glatzel,[1*]

[1] European Synchrotron Radiation Facility (ESRF) 6 Rue Jules Horowitz, BP 220 38043 Grenoble Cedex 9 France
[2] Department of Inorganic, Physical and Materials Chemistry, INSTM Reference Center and NIS Centre of Excellence, Università di Torino, Via P. Giuria 7, I-10125 Torino, Italy.
[3] Sciences Chimiques de Rennes - UMR 6226, Matériaux Inorganiques: Chimie Douce et réactivité, Université de Rennes 1, Campus de Beaulieu, Bât 10B, F-35042 Rennes, France.

Abstract
We present an application of valence to core X-ray emission spectroscopy to understand the electronic structure of the industrially relevant catalysts titanium silicalite-1. The experimental spectrum was modelled within density functional theory, adopting a one electron approach, investigating the effects of different basis sets, density functionals and cluster sizes. The description of titanium silicalite-1 valence states follows the Kohn-Sham evaluation of the molecular orbitals involved in the computed transitions.

1 Introduction

The relevance of X-ray emission spectroscopy (XES) in the fields of chemistry and material science for the investigation of the ligand environment of 3d transition metals (TM) is well reported.[1-6] We provide in the following a brief review.
XES can be induced as a second order optical process (photon-in/photon-out): (i) a core electron is removed by an incident photon, then (ii) the inner shell vacancy is filled by an electron from a higher shell following the selection rules for radiative transitions. When the core hole is filled by an electron from a valence level, we refer to valence to core XES (VtC-XES). The formal VtC-XES final state electronic configuration (i.e. hole in the valence band) is identical to the one reached by valence electron photoemission spectroscopy: X-ray/ultraviolet photoemission spectroscopy (PES). PES is a photon-in/electron-out technique, frequently used for chemical characterization of surfaces. Due to the large electron cross section mostly electrons originating from the superficial layers can leave the material. Furthermore PES is commonly performed in ultra high vacuum (UHV) conditions. The UHV restriction can be overcome with pressure up to mbars and high kinetic energy PES allows for depth profiling.
XES, in the hard X-ray range, is a truly bulk sensitive technique and is readily performed in ambient or even high pressure conditions. Furthermore, XES is an element selective tool, i.e. only electron density at the metal site (ligands included) is probed. The theoretical interpretation was shown to be surprisingly simple.[7,8]
The VtC-XES spectrum, also referred to as Kβ satellite lines, splits into the Kβ" (also called cross-over peak) and $K\beta_{2,5}$ regions, that arise from transitions involving orbitals that are primarily located on the metal centre ligands and so directly reflect the configuration of the electron orbitals that participate in the chemical bonds.[9, Glatzel, 2005 #132]
The applicability and thus importance of VtC-XES is due to the fact that it does not strictly require synchrotron radiation facilities, but can be performed using laboratory X-ray sources, radioactive isotopes[10-12] and ion beam[13] laboratory sources. It is well established that the obtained spectra can be interpreted by means of density functional theory (DFT) calculations within a one electron approximation[2,4,5,14] where no full multiplet structure,[15] core hole potential and multi-electronic processes[7] (shake-up/down) are taken into account. The chosen basis set and density functional influence the shape of the DFT computed VtC-XES spectrum.
We investigated the occupied valence molecular orbitals of the catalyst Ti silicalite-1[16] (TS-1). We present a systematic study of the effect of different basis sets, density functionals and cluster sizes used to mimic the

[1] Corresponding authors: carlo.lamberti@unito.it, pieter.glatzel@esrf.fr

Ti(IV) environment in TS-1. TS-1 is an active and selective catalyst[17-19] having H_2O_2-H_2O solution as oxidation agent, which is used in industrial plants by worldwide companies as e.g. Eni (Italy), Sumitoimo (Japan) and BASF (Germany). TS-1 belongs to the class of the so-called zeotype materials,[19] where the pure zeolite crystalline structure (i.e. where silicates are linked through oxygen atoms producing a network of three dimensional channels of molecular dimensions) has been modified by the introduction of other elements, such as transition metals, into the framework. TS-1 has the silicalite-1 structure, which is IUPAC classified as mordenite framework inverted (MFI),[20] see Figure 1a. The MFI structure has selective reaction channels whose activity depends on the Ti(IV) ions incorporated (by up to 3 wt.%) inside the framework, substituting Si in tetrahedral sites, see Figure 1b.

The confinement of a metal species in the well-defined MFI pore system gives TS-1 shape-selective properties analogous to enzymes.[21] The introduction of Ti(IV) ions inside the framework changes the chemical properties and reactivity, which has been widely studied (for a review see ref.[18]), via different spectroscopic techniques including IR,[22-24]Raman,[25,26] resonant Raman,[27-30] photoluminescence,[31] UV-Visible,[24,27,28,32-38] XAFS,[24,31,34,38-42] and neutron[43-45] and synchrotron radiation X-ray[46,47] powder diffraction, alongside theoretical[23,24,28,48-55]approaches. The studies in this field are very active because TS-1-catalysed processes are advantageous from an economical and environmental point of view pushing towards new spectroscopic and theoretical studies to solve unanswered questions about the reactivity, and so the valence states, of the metal centre in the framework. This work fills the gap in the literature of TS-1 investigating the occupied electronic levels just below the Fermi energy, coupling DFT calculations with a detailed XES study.

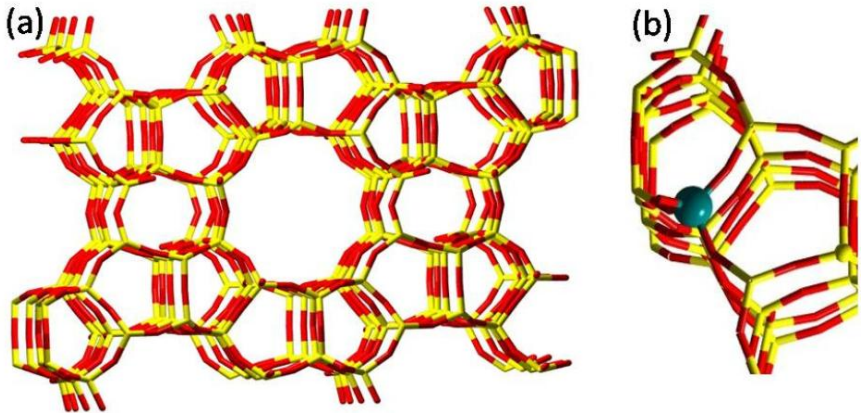

Figure 1. (a) Stick representation of MFI framework of silicalite-1 view along [010] direction. Si atoms are shown in yellow, O atoms in red. (b) Schematic representation of Ti(IV) insertion in the MFI framework. The Ti atom is reported in green.

2 Experimental

2.1 Large Scale Facility

The VtC-XES experiment was performed at the high brilliance X-ray spectroscopy beamline ID26 at the European Synchrotron Radiation Facility (ESRF, France). The incident energy was selected at 5015 eV (which is above the Ti K-edge at 4966 eV) by means of a pair of cryogenically cooled Si(311) single crystals. Higher harmonics were suppressed by three Si mirrors operating in total reflection. The sample was placed inside an ad-hoc in-situ cell oriented at 45° with respect to the incident beam and the X-ray spectrometer crystals. The beam size on the sample was approximately 0.8 mm horizontally and 0.2 mm vertically. The spectrometer exploits the Ge(331) Bragg reflection of five spherically bent analyzer crystals (radius 1000mm) arranged in a vertical Rowland circle geometry. The emitted photons were detected using an avalanche photo-diode. The resulting total energy resolution was 1.0 eV (as determined from the full width at half maximum (FWHM) of the elastically scattered peak). The Kβ satellite lines are superimposed to the $K\beta_{1,3}$ peak tail.[56] The background was subtracted by fitting four Voigt line profiles approximating the $K\beta_{1,3}$ tail. Because of the weak intensity of the Kβ satellite lines the subtraction of the background introduces an error in the resulting spectra. To estimate the error the fit procedure was performed using ten different sets of starting values. The fit average was chosen to model the main line tail.

2.2 Sample Preparation

The TS-1 sample was supplied by ENI, Instituto G. Donegani (Novara, Italy). The Ti loading was 2.76 wt%, as determined by the cell volume expansion,[46] and the absence of extra phases of TiO2 was carefully verified using Raman, UV-Vis and XANES spectroscopies. TS-1 was measured in the form of a self-supported pellet after degassing at 400 °C inside an ad-hoc X-ray fluorescence cell in order to prevent rehydration during measurement. No radiation damage (monitored by XANES and UV-Vis) was observed during the measurement.

3 Theoretical

DFT calculations were performed within the one electron approximation using the ORCA 2008 code.[57] We show, for the case of TS-1, the effects induced by using different density functionals, basis sets and cluster sizes on the computed VtC-XES spectrum.

The tested density functionals belong to different levels of the Jacob's ladder:[58] (i) local and gradient corrected (LDA, BP86, BLYP, GLYP, PBE and PWP), (ii) hybrid (like B1LYP, B3LYP, O3LYP, X3LYP, B3P, PBE0), (iii) meta GGA (TPSS), (iv) meta-hybrid GGA (TPSSh) and (v) double hybrid (B2PLYP).[57,59-62] The investigation was performed by using different standard constricted basis sets styles for all the functionals: Pople-like[63-71] (i.e. STO-3G, 3-21G, 6-31G, 6-311G), Dunning[72-77] (i.e. cc-pVDZ, cc-pVTZ, cc-pCVDZ, cc-pCVTZ, cc-pCVQZ, cc-pCV5Z, cc-pCV6Z), Ahlrichs[78-82] (i.e. SV, SVP, TZV, TZVP, QZVP, DZ, DZP, Def2-SVP, Def2-TZVP, Def2-TZVPP, Def2-QZVPP) and ANO[57] (i.e. ano-pVDZ, ano-pVTZ, ano-pVQZ, BNANO-DZP, BNANO-TZ2P, BNANO-TZ3P).[57] The computed VtC-XES spectra are reported with the maximum of the Kβ" at 0 eV. This choice is due to the different absolute emission energy error provided by different levels of theory and allows direct comparisons between the computed spectra. The only exception to this choice concerns the spectra reported in Section 4.3 (Figure 9) that are computed using the same density functional and basis sets, where all the reported spectra are computed at the same level of theory. In that case the energy origin is set to the maximum of the Kβ main line.

TS-1 is a micro-porous crystalline material and therefore both a cluster and a periodic approach may be used. We have chosen to present the calculation of the electronic structure of Ti(IV) centres in TS-1 on the basis of simple cluster models with increasing complexity including up to five tetrahedral centres (T) that mimic a fragment of the Ti-zeotype material (see Figure 1b). The investigated clusters, shown in Figure 2, are $Ti(OH)_4$, $Ti[OSiH_3]_4$ and $Ti[OSi(OH)_3]_4$ hereafter denoted T1, T5 and T5OH, respectively. The adopted nomenclature indicates the number of T-like centres (1 or 5) and in the case of clusters with five T sites, the cluster terminations (–H or –OH). A comprehensive summary of the clusters used previously to reproduce the Ti environment in TS-1 was provided by Damin et al[23] who used an ONIOM approach on clusters up to T16 and T18. In that work the authors underlined the need for big clusters in order to correctly evaluate the effect of the framework deformation in modelling the structure of molecular adsorption (H_2O and NH_3) on the Ti(IV) sites. Here we show that much smaller clusters are able to correctly reproduce the VtC-XES spectrum of degassed TS-1 due to the local probe nature of the technique. As a comparison we used a cluster of about 100 atoms containing 35 T sites (hereafter T35_MFI) directly obtained by cutting a portion of the MFI structure (see Figure 2). Twelve different T sites can be found in the MFI unit cell. As pointed out by Yuan et al,[55] a general agreement about the Ti preferential position among the T sites in the MFI framework is still missing. Marra et al[83] proposed that Ti mostly occupies T10 and T11 sites, based on low temperature X-ray diffraction, in contrast to the study of Hijar et al[44] who used neutron powder diffraction. They show that Ti was distributed among T3, T7, T8, T10 and T12 sites. Two later powder neutron diffraction studies were performed by Lamberti et al.[43] and Henry et al.[45]. Lamberti et al. showed that Ti has a tendency to occupy T11, T7 and T6 sites while Henry et al found that the most populated sites were T8, T3 and T10. The evaluation of the preferential position of the Ti atom in the framework is beyond the scope of the present work. However, twelve calculations (with optimization of the Ti position in the T35 cluster where Ti occupies one of the twelve non-equivalent positions) were performed to determine Ti-position effects on the computed VtC-XES spectra but no T dependency was observed (see the section about the cluster size effects and SI). Clusters T1, T5 and T5OH have been fully optimized using ORCA testing different levels of theory (i.e. density functionals and basis sets). For the large T35_MFI cluster, the silicate-1 geometry was adopted, obtained from neutron diffraction studies, optimizing the structure after Ti insertion in one of the cited positions, and terminating the cluster with hydrogen atoms (needed to saturate the dangling bonds at the cluster frontiers). Figure 2 and Table 1 show the results of the optimized geometries for T5 and T5OH using TPSSh as the density functional, TZVP as the basis set on all the ligand atoms and CP(PPP) on the Ti centre.

The choice to use this combination is based on TPSSh with TZVP-CP(PPP), being found to be the most appropriate combination to model the XES spectra of Ti(IV) sites in our structure (see below).
The total number of calculations performed was about 2000.

Table 1. Optimized bond distances and angles of T5 and T5OH using TPSSh as density functional and TZVP-CP(PPP) as basis sets without symmetry constrains.

	T5 bond distance (Å)	T5OH bond distance (Å)
T1-O1	1.824	1.804
T1-O2	1.827	1.802
T1-O3	1.825	1.801
T1-O4	1.826	1.799
T1-Si1	3.449	3.422
T1- Si2	3.477	3.412
T1- Si3	3.445	3.405
T1- Si4	3.485	3.408
	T5 bond angle (°)	T5OH bond angle (°)
O1-T1-O2	112.08	115.343
O1-T1-O3	114.03	114.43
O1-T1-O4	111.15	116.52
O2-T1-O3	104.07	104.10
O2-T1-O4	110.47	103.47
O3-Ti-O4	103.85	102.26

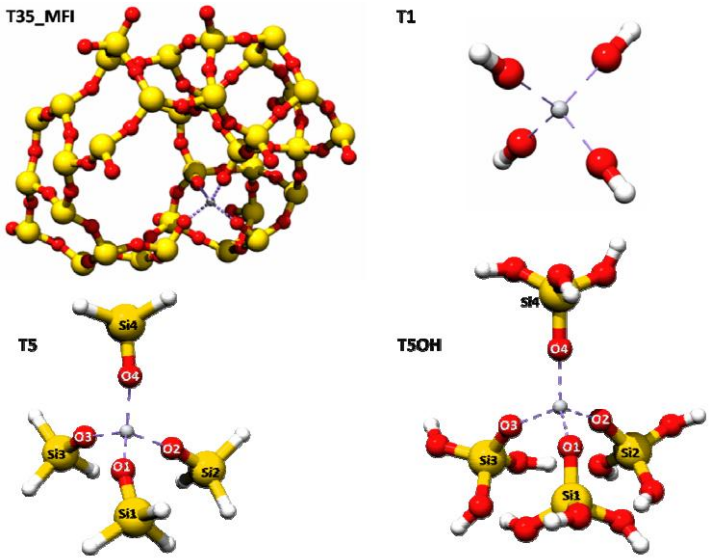

Figure 2. Clusters adopted to mimic the Ti(IV) environment in TS-1: $Ti(OH)_4$ (T1), $Ti[OSiH_3]_4$ (T5), $Ti[OSi(OH)_3]_4$ (T5OH) and T35_MFI (terminal H atoms not reported for simplicity). In red, yellow, gray and white are reported respectively O, Si, Ti and H atoms. Labels have been inserted for T5 and T5OH to allow the definitions of bond distances and angles.

4 Results and Discussion

Figure 3a shows the non-resonant Kβ X-ray emission lines of degassed TS-1. The VtC-XES spectrum (also called Kβ satellite lines) arises in the region between 4935 to 4970 eV superimposed on the $K\beta_{1,3}$ tail. For a quantitative comparison between experiment and calculation the background was fitted using four Voigt functions. The background-removed VtC-XES spectrum is shown in the inset of Figure 3a. A first moment analysis (FMA) was then applied to estimate the energy "centre of mass" (E_{cm}) of Kβ" and $K\beta_{2,5}$ using the following formula:

$$E_{cm} = \frac{\sum_i^n I_i E_i}{\sum_i^n I_i}$$

where I_i and E_i are the i^{th}-point intensity and energy, respectively of the fitted Kβ"(A in Figure 3b) and $K\beta_{2,5}$ (D+B+C, in Figure 3b). The obtained E_{cm} values for Kβ" and $K\beta_{2,5}$ were 4946.0 ± 0.1 eV and 4959.8 ± 0.1

eV hereafter, respectively called $E_{cm}(K\beta'')$ and $E_{cm}(K\beta_{2,5})$. The difference (ΔE_{cm}=18.2±0.2 eV) between $E_{cm}(K\beta'')$ and $E_{cm}(K\beta_{2,5})$ and the difference (ΔE_{max}=13.2±0.1 eV) between the maximum of the peak labelled A and B in Figure 3b were used as figure of merit to evaluate the discrepancy between the experiment and the calculations. The analysis performed on the whole set of calculations showed that the best compromise between the computational time and the chosen figure of merit values is achieved using TPSSh density functional, adopting the TZVP basis set to treat the metal ligands and the CP(PPP) basis set for the Ti atom, on the T5OH cluster structure. For this reason the discussion of the effect of different basis set is reported, in Section 4.1, using the TPSSh functional and the T5OH cluster only. The effect of different density functional is discussed in Section 4.2, using the cluster T5OH, choosing the CP(PPP) basis set for Ti and TZVP for the ligand atoms. Analogously, in Section 4.3, the effect of the cluster size is investigated only for calculations performed using TPSSh as density functional and CP(PPP) (Ti)/TZVP(ligands) basis sets. A brief discussion about the core hole potential effect is given in Section 4.4.

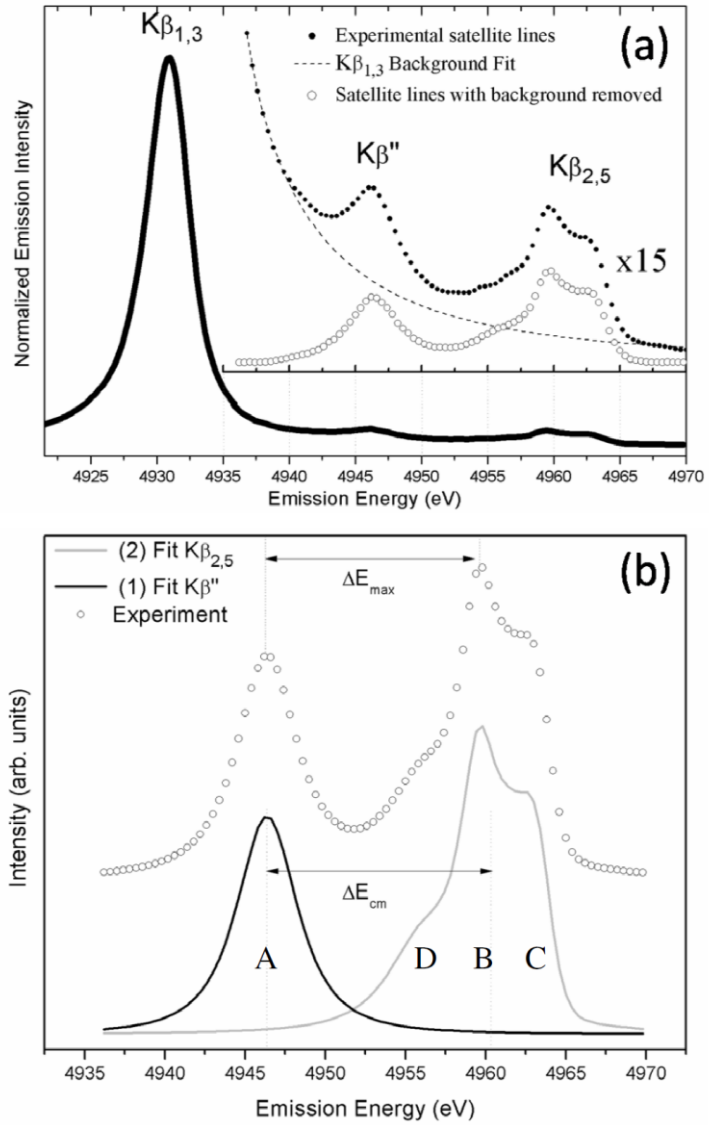

Figure 3 (a): Kβ line (solid line) for TS-1. Inset: VtC-XES spectrum (full circle), fit to the $K\beta_{1,3}$ tail (dashed line), background removed VtC-XES lines (open circle). (b): Experimental background-removed VtC-XES spectrum (top open circle) as in (a). Fit of the Kβ" and $K\beta_{2,5}$ regions, black and gray curves respectively

4.1 Basis Set Effects

Figure 4 and 5 report the computed VtC-XES spectra, based on the T5OH cluster, using the TPSSh functional for a selection of basis sets, adopting the convolution parameter suggested in literature.[4] The spectral features were normalized in peak and shifted to have the maximum of the Kβ" at 0 eV. In all the computed spectra four main features are observed: A, B, C and D.

Figure 4a shows a selection of four Pople-like basis sets (STO-3G, 3-21G, 6-31G and 6-311G). STO-3G is a minimal basis set, largely applied in the past to treat fourth and fifth-row elements.[84] This basis set was so popular due to its ability to correctly predict geometries. This ability, however, comes from the large super-position error that partially cancels other defects producing reasonable bond length.[85] As visible from Figure 4a the STO-3G spectrum presents an incorrect intensity trend in the $K\beta_{2,5}$ region: the intensities of B and C are inverted compared with the experiment (cfr Figure 3). Furthermore, the values of ΔE_{max} and ΔE_{cm} are about 1 eV larger than the experimental values. 3-21G belongs to the class of the so called split valence basis sets (SVBS). The resulting ΔE_{max} and ΔE_{cm} are 14.9 eV and 13.6 eV respectively, with the intensity of C overestimated by about 30%. In the whole set of the tested basis 3-21G was the fastest. For this reason the reported CPU times (see Figure 6) are normalized to the one of 3-21G. Moving to the 6-31G basis set the number of primitive devoted to the core and first valence function increases together with the CPU time without improvement for ΔE_{max} and ΔE_{cm}. The computed spectrum does not undergo any significant modification compared with the case of 3-21G while the CPU 18-fold increases. On the contrary the single zeta core, triple zeta valence and polarization function basis set 6-311G was able to qualitatively reproduce the intensity trend between B and C, but it overestimates the intensity of A of about 15% with respect the experimental finding. The values of ΔE_{max} and ΔE_{cm} for this basis set are respectively 13.5 eV and 14.3 eV. 6-311G is 24-fold times CPU demanding than 3-21G but provides the best results inside the tested Pople-like basis set family.

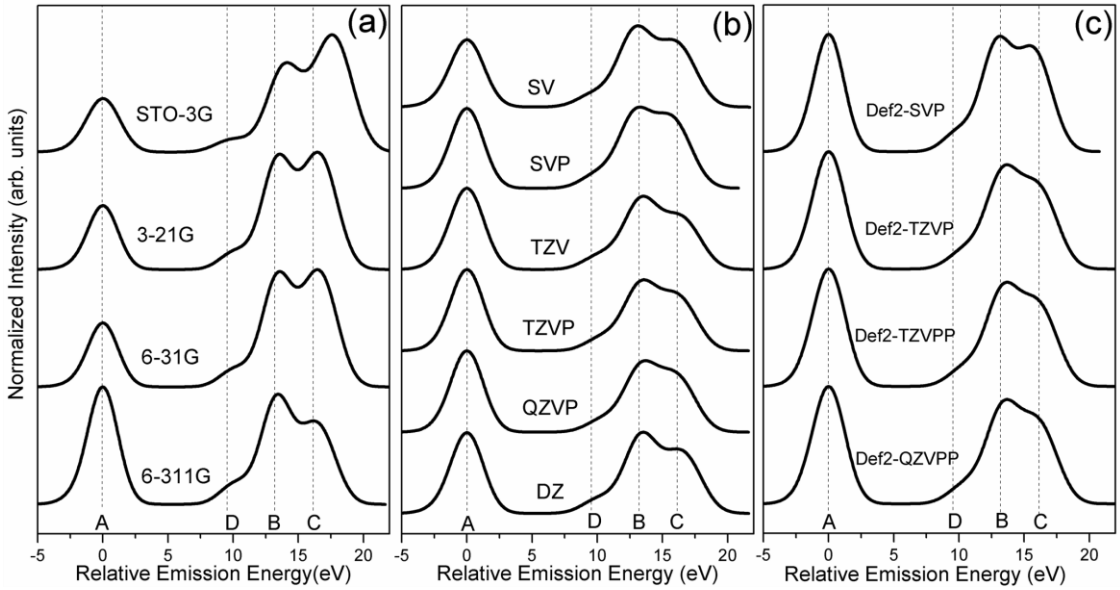

Figure 4. VtC-XES spectra computed adopting TPSSh functional on T5OH cluster of different basis sets. (a): Selection of Pople-like basis sets. (b) and (c): Selection of Ahlrichs-like basis sets. The spectral features were normalized to the unit at the point of maximum intensity and then energy shifted to have the maximum of the Kβ" peak as zero.

Ahlrichs-like SVBS with and without polarization functions are shown in Figure 4b. The intensity of A is overestimated for all the members of this group of basis sets. The only basis set that qualitatively reproduce the intensity trend between A, B and C is the SV. However also for SV the calculated A intensity is 10% more intense than the experimental one. The values of the figure of merit, ΔE_{max} and ΔE_{cm}, are overestimated by about 3% from all the members of this family. We would like to underline that SVP, TZVP, QZVP overestimate the C:B intensity ratio by about 25%. Summarizing we found that the Ahlrichs basis sets gives results comparable with 6-311G requiring more CPU time (see Figure 6).

As expected, moving to Def2-Ahlrichs family basis sets (Figure 4c), the same general agreement encountered above for the Ahlrichs-group is reached, with the values of the figure of merit, ΔE_{max} and ΔE_{cm}, overestimated by about 3%. As a general result we found that all the Def2 basis sets overestimate the Kβ" intensity by about 25%. We would underline that the less demanding Def2-SVP yields better values for ΔE_{max} and ΔE_{cm} inside the Def2-group (see Figure 6).

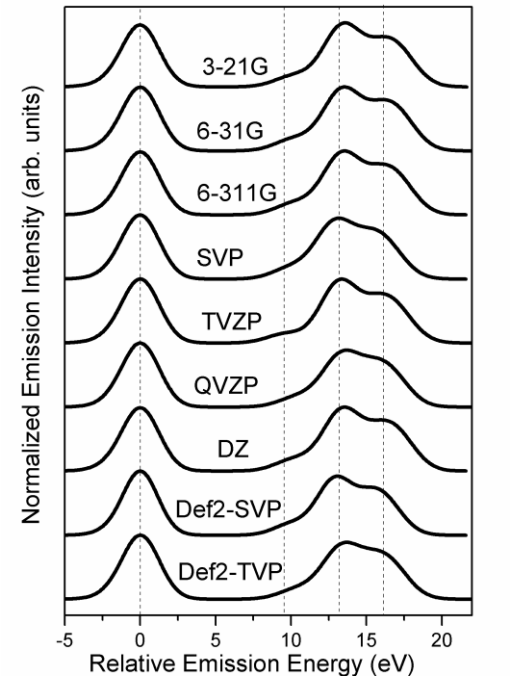

Figure 5. VtC-XES spectra computed adopting TPSSh functional on T5OH cluster of different basis sets, fixing in all cases the basis set of the Ti atom to CP(PPP) and changing the basis set on the ligand atoms. The spectral features were normalized to the unit at the point of maximum intensity and then energy shifted to have the maximum of the Kβ" peak as zero. The adopted grid for the integration is 15 for the Ti atom, 10 for O and Si atoms and 5 for the H atoms.

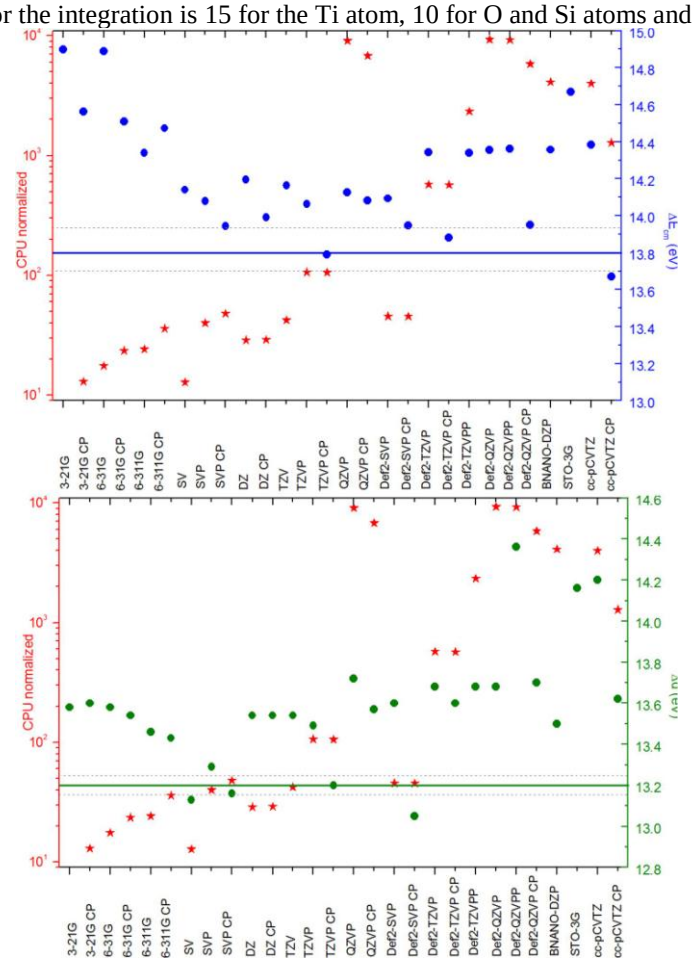

Figure 6. Top: ΔE_{cm} (blue circles, right ordinate axis) and normalized CPU time (red stars, left ordinate axis in logarithmic scale) for a selection of basis sets. The horizontal full line refer to the experimental value while the two dashed ones refer to the experimental error. Bottom: As top for ΔE_{max}. All the calculations were done using the T5OH cluster adopting the TPSSh density functional. When in the abscissa only one basis set is indicated it refers to all the atoms in the cluster. When two basis set are reported the first refers to the ligands and the later refers to Ti atom.

The previous calculations were performed using the same basis set for all the atoms in the cluster. We also considered the effect of different basis sets on O and Si. To this purpose we used the flexible CP(PPP) basis set to treat the Ti atom. The results of this investigation are shown, for a selection of basis set, in Figure 5. Firstly, we notice that using the CP(PPP) basis set on Ti, the calculated VtC-XES spectral shape (compare Figure 5 with Figure 4) together with the figure of merit values improve (see also Figure 6). Secondly, we found that Pople-like basis set produce spectra with figure of merit values closer to the experimental one moving from 3-21G to 6-311G (i.e. increasing the primitive size). However the best results were obtained inside the Ahlrichs-like basis set family. All the results of this section are summarized in Figure 6 where the corresponding ΔE_{max} and ΔE_{cm} (right axis) are reported for each basis set, together with the value of the normalized CPU time needed to perform the calculations (left axis). The latter is reported by normalizing to the unit the CPU time of the faster basis set (i.e. 3-21G). In both cases the experimental value of ΔE_{max} and ΔE_{cm} is reported as horizontal full line. The rectangle defined by the two dashed lines selects basis sets compatible within the experimental error of the figure of merit values. We conclude that the use of TZVP (ligands) and CP(PPP) (Ti) yield the best compromise between CPU time and accuracy to reproduce the TS-1 VtC-XES spectrum.

4.2 Density Functionals Effects

Figure 7 shows the theoretical VtC-XES spectra computed for the T5OH cluster using the TZVP (ligands)/CP(PPP)(Ti atom) basis set for a selection of density functionals that belong to different families: (i) local and gradient corrected (LDA, BP86, BLYP, GLYP, PBE and PWP), (ii) hybrid (B1LYP, B3LYP, PBE0), (iii) meta-gradient corrected (TPSS), (iv) meta-hybrid gradient corrected (TPSS0, TPSSh) and (v) double hybrid (B2PLYP). The figure of merit values are reported in Figure 8. The intensity trend in the $K\beta_{2,5}$ region is well reproduced by all the density functionals. We would underline however that the intensity of the Kβ" peak is overestimated by about 25% by all the tested density functional (cfr Figure 7 with Figure 3). Regarding the figure of merit values: ΔE_{cm} is well reproduced only by PBE, TPSS and TPSSh. The last one (TPSSh) reproduces exactly the experimental value, represented as blue line in Figure 8a. ΔE_{max} is well reproduced by B3LYP, TPSS and TPSSh. Again, TPSSh provides the exact experimental value, represented as green line in Figure 8b. We found that a functionals that depend on the kinetic energy density like TPSS produce results comparable with B3LYP, while the introduction of 10% of the exact exchange functional, i.e. using TPSSh, improves the calculations. We concluded that TPSSh is the best choice (between the tested functionals) to calculated VtC-XES spectra for systems like TS-1.

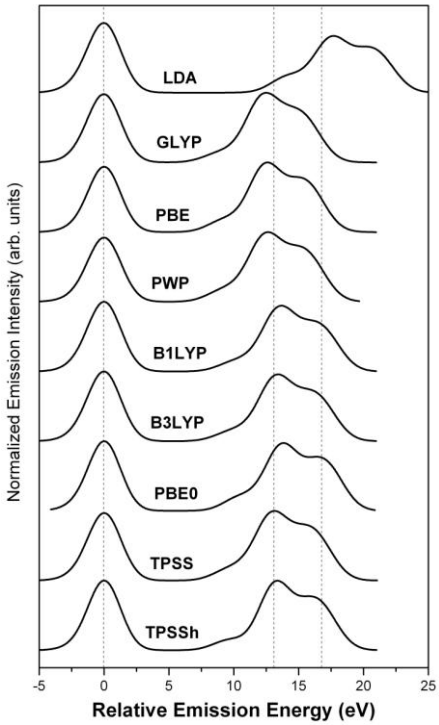

Figure 7. Selection of VtC-XES spectra computed for the T5OH cluster using different density functionals. The basis sets used were TZVP for ligands and CP(PPP) for Ti.

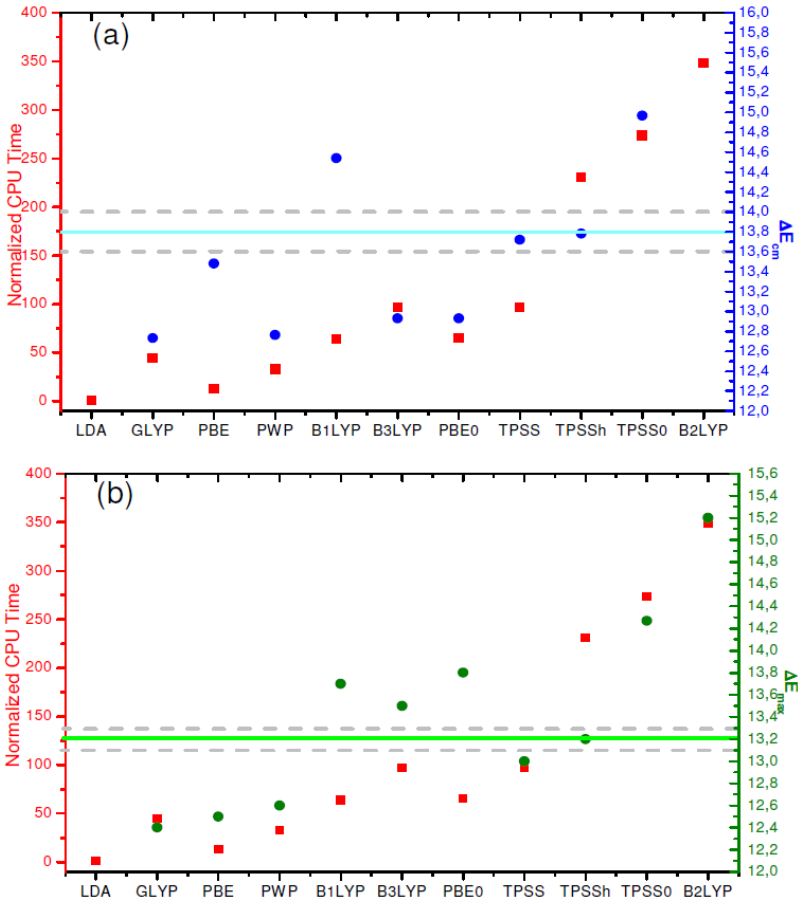

Figure 8. Top: ΔE_{cm} (blue circles, right ordinate axis) and normalized CPU time (red stars, left ordinate axis in logarithmic scale) for a selection of density functionals. The horizontal full line refer to the experimental value while the two dashed ones refer to the experimental error. Bottom: As top for ΔE_{max}. All the calculations were done using the T5OH cluster adopting the TZVP(ligands) and CP(PPP) (Ti) basis sets. The numerical values for ΔE_{max} and ΔE_{cm} are reported in Table S1 of the SI.

4.3 Cluster Size Effects

The spectra (normalized in peak maximum) computed using the cluster T1, T5, T5OH and T35_MFI (Ti in T11) are shown in Figure 9a, respectively in green, blue, red and gray. All the calculations were performed using the same functional (TPSSh) and basis sets (TZVP, CP(PPP)). The choice to compute T35_MFI with Ti in T11 position is arbitrary: the VtC-XES spectrum was found to be T-independent (see Figure S1 of the SI). Three main spectral features A, B and C are observed for all the spectra in Figure 9a, showing a cluster size depending fine structure, while the features labelled D arise only for T5OH and T35_MFI. In general the molecular orbitals (MOs) linked to transitions responsible for A have strong O (first shell) 2s atomic character (labelled a in Figure 9b,c,d,e). In particular, in the case of T1, the MOs responsible for A are degenerate, see Table 2 and Figure 9b. Increasing the cluster size, moving to T5, T5OH and T35_MFI the degeneracy is removed and new small contribution are revealed in the lower energy part of the spectra. The involved MOs present Si 3s and, in the case of T5OH and T35_MFI, O (third shell) 2s atomic character. Unlikely the contributions to A, the features labelled B and C arise from transitions involving MOs with mainly O(first shell) 2p atomic character. The main difference between B and C is that while the MOs characterizing B have mainly σ character the MOs characterizing C have mainly π character. As said at the beginning, only T5OH and T35_MFI show the shoulder D (see Figure 9d,e and Table 2), that is mainly due to MOs localized on the SiO_4 groups (see also Figure 3). Furthermore, from a direct comparison between Figure 9d (T5OH) and Figure 9e (T35_MFI), we see that no significant spectral shape modifications occur when increasing the cluster size up to 35 T-centres. For this reason we do think that the VtC-XES spectrum of degassed TS-1 can be modelled taking into account the coordination of one Ti atom including ligands up to the third coordination shell (T5OH cluster). The atomic compositions of the MOs linked to the transitions that strongly contribute to the spectra of T1, T5 and T5OH are summarized in Table 2.

Table 2. Key molecular orbital contributions of the VtC-XES spectra computed on cluster T1, T5 and T5OH, using TPSSh as density functional and TZVP/CP(PPP) as basis sets.

T1 Cluster

MO	Energy(eV)	Ti(3*p*) %	Ti(3d) %	1st shell ligands	
				O(2*s*) %	O(2*p*) %
a	15.6	6.3	4.5	80.2	0.1
b	27.9	3.2	14.1	0.6	74.2
c	32.4	6.5	6.4	0.1	78.5

T5 Cluster

MO	Energy(eV)	Ti(3*p*) %	Ti(3d) %	1st shell ligands		2nd shell ligands	
				O(2*s*) %	O(2*p*) %	Si(3*s*)%	Si(3*p*)%
a	15.3	6.7	5.3	70.6	0.1	4.6	5.1
b	27.1	2.1	7.5	0.0	46.4	23.6	0.4
c2	30.0	1.5	10.5	0.0	25.6	2.4	16.8
c1	30.8	4.7	1.0	0.0	57.1	0.2	20.7
c3	33.0	1.7	2.0	0.0	13.5	0.0	19.2

T5OH Cluster

MO	Energy(eV)	Ti(3*p*) %	Ti(3d) %	1st shell ligands		2nd shell ligands		3rd shell ligands	
				O(2*s*) %	O(2*p*)%	Si(3*s*)%	Si(3*p*)%	O(2*s*)%	O(2*p*)%
a	15.1	9.8	4.4	61.5	0.3	2.2	7.1	2.0	0.0
b	28.2	3.1	11.3	0.7	52.6	2.1	10.5	0.8	14.6
c	30.6	0.4	4.5	0.3	11.2	0.0	5.3	1.3	39.7
c1	32.2	0.3	1.2	0.0	9.8	0.0	0.9	0.7	53.3
d	25.1	1.0	0.5	0.5	23.6	17.2	1.4	2.6	42.4

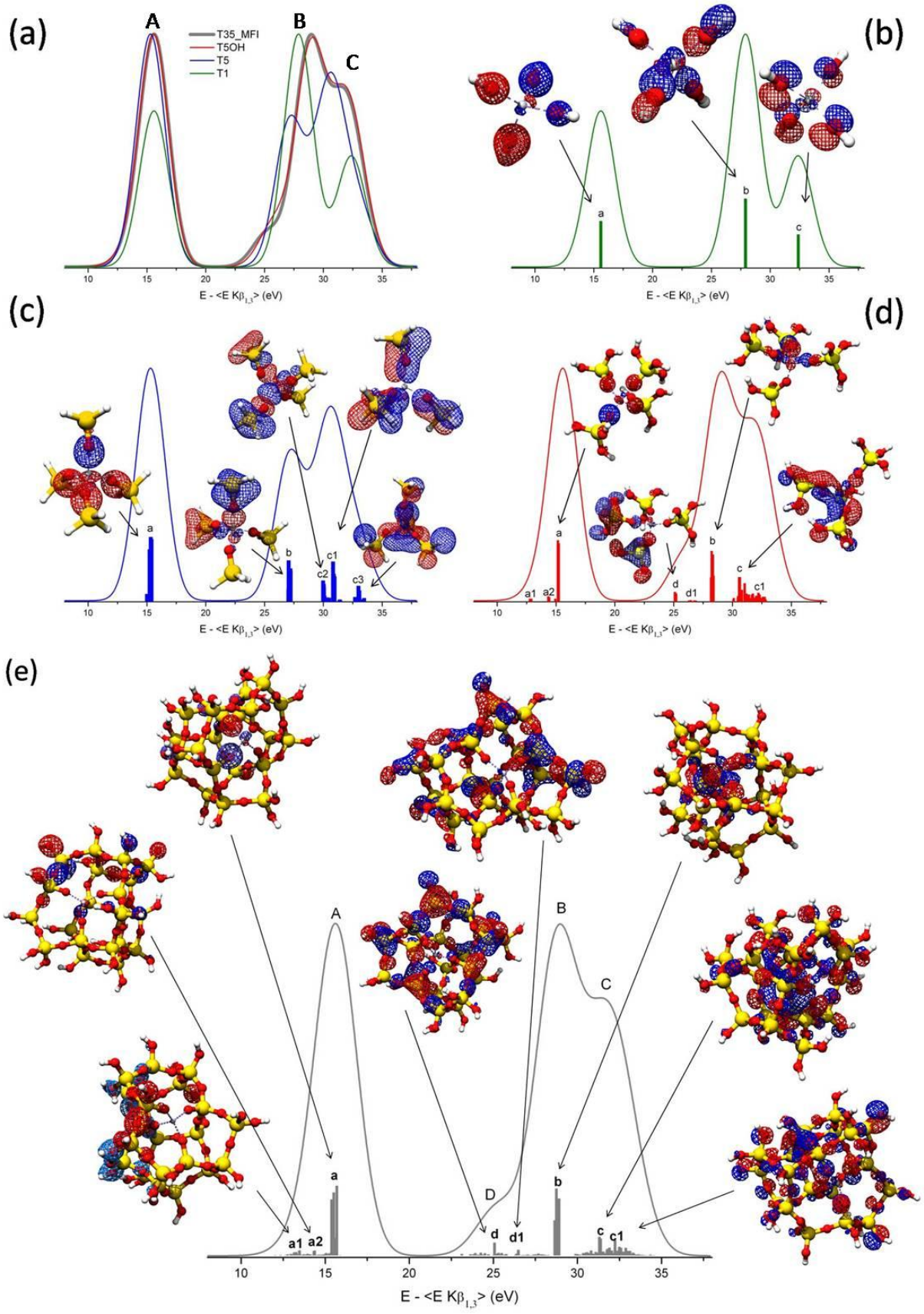

Figure 9. (a) VtC-XES spectra computed on T1 (green), T5 (blue), T5OH (red) and T35_MFI (gray) cluster adopting TPSSh/TZVP/CP(PPP) level of theory. (b),(c), (d) and (e) show VtC-XES spectra for T1, T5, T5OH and T35_MFI with the most relevant MOs.

4.4 Z+1 Approach

As noticed in the previous section the Kβ" intensity is consistently overestimated. This effect can be linked to the used approximations that, among other mechanisms do not take into account the core hole potential. We explored the effect of the core hole potential arising from the photo-ionization, modifying the T5OH cluster. We substituted Ti with a V atom without re-optimizing the cluster, to simulate the effective nuclear charge in presence of a 1s core hole (Z+1 model). The core hole lifetime is on the order of one fs which is too short for significant structural rearrangement. The energy scales have been shifted such that they coincide in the Kβ" peak position. The comparison between Ti-T5OH (red) and V-T5OH (grey) is shown in Figure 10. The V-T5OH Kβ" line has an intensity of about 18% lower than Ti-T5OH, living better agreement with the experimental data. At the same time however the $K\beta_{2,5}$ peak changes: C decreases in intensity by 2% compared with Ti-T5OH, but still in agreement with the experimental data. We found that the most import modifications between the spectra computed using Ti-T5OH and V-T5OH are obtained in the Kβ" region that arises from transition involving molecular orbitals closer to the nucleus than the ones involved in the transitions giving rise $K\beta_{2,5}$.

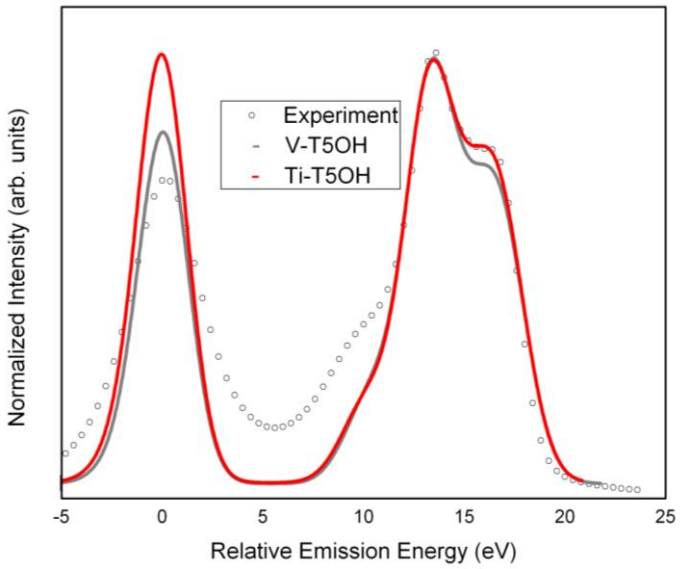

Figure 10. Calculated spectra adopting TZVP-CP(PPP) at the TPSSh level of theory on the T5OH cluster. Ti-T5OH Kβ satellite lines (red) are compared with the Kβ satellite lines computed substituting the metal centre with V without optimization. For comparison the experimental spectrum is reported represented as scattered circles.

5 Conclusions

The occupied valence molecular orbitals of TS-1 were investigated by means of valence to core X-ray emission spectroscopy. The spectral features were interpreted using DFT calculations, adopting the ORCA 2008 package. We tested a large number of basis sets (30) and density functionals (16) on clusters of increasing size around the Ti atom. The best agreement between calculation and experiment was achieved adopting the T5OH cluster with 25 atoms using the TPSSh density functional with a standard polarized triple ζ basis set (TZVP) on Si and O atoms, and the CP(PPP) basis set on Ti. A larger cluster (T35_MFI) was used to compute the VtC-XES spectra and no significant improvement was observed as compared to T5OH. We believe that our findings generally apply to VtC-XES on 3d TM metals. First calculations on Co and Cu containing systems confirm this statement.

Acknowledgements

We wish to thank K. Kvashnina, M. Rovezzi, Y. Kvashnin, C. Lapras (ESRF) and F. Bonino, D. Gianolio, A. Piovano, (University of Torino) for the support during the experiment and discussions. J. Swarbrick (ESRF), S. Bordiga and A. Damin (University of Torino) are acknowledged for a critical reading of the manuscript. The support provided by C. Ferrero and R. Wilcke (ESRF, ISDD/Scientific Software Group) is gratefully acknowledged.

Text for the table of contents

XES supported by DFT reveals the valence molecular orbital composition of Ti centres in TS-1.

Figure for the table of contents

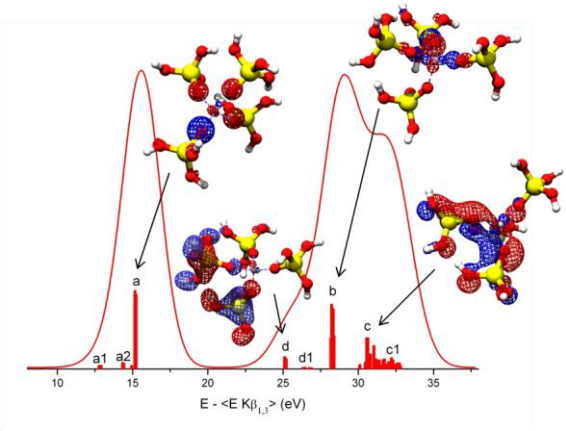

References

1 U. Bergmann and P. Glatzel, *Photosynthesis Research*, 2009, **102**, 255.
2 G. Smolentsev, A. V. Soldatov, J. Messinger, K. Merz, T. Weyhermuller, U. Bergmann, Y. Pushkar, J. Yano, V. K. Yachandra and P. Glatzel, *J. Am. Chem. Soc.*, 2009, **131**, 13161.
3 V. A. Safonov, L. N. Vykhodtseva, Y. M. Polukarov, O. V. Safonova, G. Smolentsev, M. Sikora, S. G. Eeckhout and P. Glatzel, *J. Phys. Chem. B*, 2006, **110**, 23192.
4 J. C. Swarbrick, Y. Kvashnin, K. Schulte, K. Seenivasan, C. Lamberti and P. Glatzel, *Inorg. Chem.*, 2010, **49**, 8323.
5 N. Lee, T. Petrenko, U. Bergmann, F. Neese and S. DeBeer, *J. Am. Chem. Soc.*, 2010, **132**, 9715.
6 S. G. Eeckhout, O. V. Safonova, G. Smolentsev, M. Biasioli, V. A. Safonov, L. N. Vykhodtseva, M. Sikora and P. Glatzel, *J. of Anal. Atomic Spectrom.*, 2009, **24**, 215.
7 F. de Groot and A. Kotani, *Core Level Spectroscopyof Solids*; CRC Press, **2008**; Vol. 6.
8 P. Glatzel, M. Sikora, S. G. Eeckhout, O. V. Safonova, G. Smolentsev, G. Pirngruber, J. A. van Bokhoven, J. D. Grunewaldt and M. Tromp, *Synchrotron Radiation Instrumentation, Pts 1 and 2*, 2007, **879**, 1731.
9 U. Bergmann, C. R. Horne, T. J. Collins, J. M. Workman and S. P. Cramer, *Chem. Phys. Lett.*, 1999, **302**, 119.
10 P. Glatzel, U. Bergmann, F. M. F. de Groot and S. P. Cramer, *Physical Review B*, 2001, **6404**.
11 P. Glatzel, U. Bergmann, F. deGroot and S. P. Cramer, *Abstr. Pap. Am. Chem. Soc.*, 2000, **219**, U841.
12 U. Bergmann, P. Glatzel, F. deGroot and S. P. Cramer, *J. Am. Chem. Soc.*, 1999, **121**, 4926.
13 L. Mandic, S. Fazinic and M. Jaksic, *Physical Review A*, 2009, **80**.
14 S. D. George, T. Petrenko and F. Neese, *J. Phys. Chem. A*, 2008, **112**, 12936.
15 F. de Groot, *Chem. Rev.*, 2001, **101**, 1779.
16 M. Taramasso, G. Perego and B. Notari, **1983**, US Patent No. 4410501.
17 B. Notari, *Adv. Catal.*, 1996, **41**, 253.
18 S. Bordiga, F. Bonino, A. Damin and C. Lamberti, *Phys. Chem. Chem. Phys.*, 2007, **9**, 4854.
19 A. Corma, *J. Catal.*, 2003, **216**, 298.
20 W. M. Meier, D. H. Olson and C. Baerlocher, *Atlas of Zeolite Structure Types*; Elsevier: London, **1996**.
21 R. A. Sheldon, *Stud. Surf. Sci. Catal.*, 1997, **110**, 151.
22 M. A. Camblor, A. Corma and J. Perezpariente, *Chem. Commun.*, 1993, 557.
23 A. Damin, S. Bordiga, A. Zecchina and C. Lamberti, *J. Chem. Phys.*, 2002, **117**, 226.
24 S. Bordiga, A. Damin, F. Bonino, A. Zecchina, G. Spanò, F. Rivetti, V. Bolis and C. Lamberti, *J. Phys. Chem. B*, 2002, **106**, 9892.
25 D. Scarano, A. Zecchina, S. Bordiga, F. Geobaldo, G. Spoto, G. Petrini, G. Leofanti, M. Padovan and G. Tozzola, *J. Chem. Soc. Faraday Trans.*, 1993, **89**, 4123.
26 G. Deo, A. M. Turek, I. E. Wachs, D. R. C. Huybrechts and P. A. Jacobs, *Zeolites*, 1993, **13**, 365.
27 C. Li, G. Xiong, Q. Xin, J. Liu, P. Ying, Z. Feng, J. Li, W. Yang, Y. Wang, G. Wang, X. Liu, M. Lin, X. Wang and E. Min, *Angew. Chem. Int. Ed.*, 1999, **38**, 2220.
28 G. Ricchiardi, A. Damin, S. Bordiga, C. Lamberti, G. Spanò, F. Rivetti and A. Zecchina, *J. Am. Chem. Soc.*, 2001, **123**, 11409.
29 S. Bordiga, A. Damin, F. Bonino, G. Ricchiardi, C. Lamberti and A. Zecchina, *Angew. Chem. Int. Ed.*, 2002, **41**, 4734.
30 S. Bordiga, A. Damin, F. Bonino, G. Ricchiardi, A. Zecchina, R. Tagliapietra and C. Lamberti, *Phys. Chem. Chem. Phys.*, 2003, **5**, 4390.
31 C. Lamberti, S. Bordiga, D. Arduino, A. Zecchina, F. Geobaldo, G. Spanò, F. Genoni, G. Petrini, A. Carati, F. Villain and G. J. Vlaic, *Phys. Chem. B*, 1998, **102**, 6382.
32 A. Zecchina, G. Spoto, S. Bordiga, M. Padovan and G. Leofanti, *Stud. Surf. Sci. Catal.*, 1991, **65**, 671.
33 T. Blasco, M. Camblor, A. Corma and J. Pérez-Parriente, *J. Am. Chem. Soc.*, 1993, **115**, 11806.

34 S. Bordiga, S. Coluccia, C. Lamberti, L. Marchese, A. Zecchina, F. Boscherini, F. Buffa, F. Genoni, G. Leofanti, G. Petrini and G. Vlaic, *J. Phys. Chem.*, 1994, **98**, 4125.
35 T. Trong On, A. Bittar, A. Sayari, S. Kaliaguine and L. Bonneviot, *Catal. Lett.*, 1992, **16**, 85.
36 T. Trong On, L. Bonneviot, A. Bittar, A. Sayari and S. Kaliaguine, *J. Mol. Catal.*, 1992, **74**, 233.
37 G. N. Vayssilov, *Catal. Rev.-Sci. Eng.*, 1997, **39**, 209.
38 F. Bonino, A. Damin, G. Ricchiardi, Ricci M, Spanò G, D'Aloisio R, Zecchina A, Lamberti C, Prestipino C and S. Bordiga, *J. Phys. Chem. B*, 2004, **108**, 3573.
39 P. Behrens, J. Felsche, S. Vetter, G. Schulzekloff, N. I. Jaeger and W. Niemann, *J. Chem. Soc.-Chem. Commun.*, 1991, 678.
40 S. Bordiga, F. Boscherini, S. Coluccia, F. Genoni, C. Lamberti, G. Leofanti, L. Marchese, G. Petrini, G. Vlaic and A. Zecchina, *Catal. Lett.*, 1994, **26**, 195.
41 D. Gleeson, G. Sankar, C. R. A. Catlow, J. M. Thomas, G. Spanó, S. Bordiga, A. Zecchina and C. Lamberti, *Phys. Chem. Chem. Phys.*, 2000, **2**, 4812.
42 J. M. Thomas and G. Sankar, *Accounts Chem. Res.*, 2001, **34**, 571.
43 C. Lamberti, S. Bordiga, A. Zecchina, G. Artioli, G. L. Marra and G. Spanò, *J. Am. Chem. Soc.*, 2001, **123**, 2204.
44 C. A. Hijar, R. M. Jacubinas, J. Eckert, N. J. Henson, P. J. Hay and K. C. Ott, *J. Phys. Chem. B*, 2000, **104**, 12157.
45 P. F. Henry, M. T. Weller and C. C. Wilson, *J. Phys. Chem. B*, 2001, **105**, 7452.
46 C. Lamberti, S. Bordiga, A. Zecchina, A. Carati, A. N. Fitch, G. Artioli, G. Petrini, M. Salvalaggio and G. L. Marra, *J. Catal.*, 1999, **183**, 222.
47 M. Milanesio, G. Artioli, A. F. Gualtieri, L. Palin and C. Lamberti, *J. Am. Chem. Soc.*, 2003, **125**, 14549.
48 R. Millini, G. Perego and K. Seiti, *Stud. Surf. Sci. Catal.*, 1994, **84**, 2123.
49 A. Damin, G. Ricchiardi, S. Bordiga, A. Zecchina, F. Ricci, G. Spano and C. Lamberti, *Stud. Surf. Sci. Catal.*, 2001, **140**, 195.
50 A. Damin, S. Bordiga, A. Zecchina, K. Doll and C. Lamberti, *J. Chem. Phys.*, 2003, **118**, 10183.
51 E. Fois, A. Gamba and G. Tabacchi, *ChemPhysChem*, 2005, **6**, 1237.
52 A. Gamba, G. Tabacchi and E. Fois, *J. Phys. Chem. A*, 2009, **113**, 15006.
53 D. H. Wells, A. M. Joshi, W. N. Delgass and K. T. Thomson, *J. Phys. Chem. B*, 2006, **110**, 14627.
54 G. Ricchiardi, A. de Man and J. Sauer, *Phys. Chem. Chem. Phys.*, 2000, **2**, 2195.
55 S. P. Yuan, H. Z. Si, A. P. Fu, T. S. Chu, F. H. Tian, Y. B. Duan and J. G. Wang, *J. Phys. Chem. A*, 2011, **115**, 940.
56 G. Peng, F. M. F. Degroot, K. Hamalainen, J. A. Moore, X. Wang, M. M. Grush, J. B. Hastings, D. P. Siddons, W. H. Armstrong, O. C. Mullins and S. P. Cramer, *J. Am. Chem. Soc.*, 1994, **116**, 2914.
57 F. Neese, *ORCA – an ab initio, Density Functional and Semiempirical program package*; Version 2.6 ed.; University of Bonn: Bonn, **2008,** and Refs. therein.
58 J. M. Tao, J. P. Perdew, V. N. Staroverov and G. E. Scuseria, *Phys. Rev. Lett.*, 2003, **91**.
59 J. P. Perdew, K. Burke and Y. Wang, *Physical Review B*, 1998, **57**, 14999.
60 J. P. Perdew, M. Ernzerhof, A. Zupan and K. Burke, *J. Chem. Phys.*, 1998, **108**, 1522.
61 J. P. Perdew and K. Schmidt, *AIP Conf. Proc.*, 2001, **577**, 1.
62 K. P. Jensen, *Inorganic Chemistry*, 2008, **47**, 10357.
63 W. J. Hehre, Ditchfie.R, R. F. Stewart and J. A. Pople, *J. Chem. Phys.*, 1970, **52**, 2769.
64 W. J. Hehre and J. A. Pople, *J. Chem. Phys.*, 1972, **56**, 4233.
65 W. J. Hehre, Ditchfie.R and J. A. Pople, *J. Chem. Phys.*, 1972, **56**, 2257.
66 J. D. Dill and J. A. Pople, *J. Chem. Phys.*, 1975, **62**, 2921.
67 J. A. Pople and W. J. Hehre, *J. Comput. Phys.*, 1978, **27**, 161.
68 R. Ditchfie, W. J. Hehre and J. A. Pople, *J. Chem. Phys.*, 1970, **52**, 5001.
69 R. Ditchfie, W. J. Hehre and J. A. Pople, *J. Chem. Phys.*, 1971, **54**, 724.
70 R. Ditchfie, D. P. Miller and J. A. Pople, *J. Chem. Phys.*, 1970, **53**, 613.
71 R. Ditchfield, W. J. Hehre, J. A. Pople and L. Radom, *Chem. Phys. Lett.*, 1970, **5**, 13.
72 T. H. Dunning, *J. Chem. Phys.*, 1970, **53**, 2823.
73 T. H. Dunning, *Chem. Phys. Lett.*, 1970, **7**, 423.
74 T. H. Dunning, *J. Chem. Phys.*, 1971, **55**, 3958.
75 T. H. Dunning, *J. Chem. Phys.*, 1971, **55**, 716.
76 T. H. Dunning, *J. Chem. Phys.*, 1977, **66**, 1382.
77 T. H. Dunning, *J. Chem. Phys.*, 1989, **90**, 1007.
78 A. Schafer, H. Horn and R. Ahlrichs, *J. Chem. Phys.*, 1992, **97**, 2571.
79 K. Eichkorn, O. Treutler, H. Ohm, M. Haser and R. Ahlrichs, *Chem. Phys. Lett.*, 1995, **240**, 283.
80 K. Eichkorn, F. Weigend, O. Treutler and R. Ahlrichs, *Theor. Chem. Acc.*, 1997, **97**, 119.
81 F. Weigend and R. Ahlrichs, *Phys. Chem. Chem. Phys.*, 2005, **7**, 3297.
82 F. Weigend, F. Furche and R. Ahlrichs, *J. Chem. Phys.*, 2003, **119**, 12753.
83 G. L. Marra, G. Artioli, A. N. Fitch, M. Milanesio and C. Lamberti, *Microporous and Mesoporous Materials*, 2000, **40**, 85.
84 W. J. Pietro and W. J. Hehre, *J. Comput. Chem.*, 1983, **4**, 241.
85 E. R. Davidson and D. Feller, *Chem. Rev.*, 1986, **86**, 681.

SUPPORTING INFORMATION

Investigation of the valence electronic states of Ti(IV) in Ti silicalite-1 coupling X-ray emission spectroscopy and density functional calculations

Erik Gallo,[1,2,3] Carlo Lamberti,[2,3] Pieter Glatzel,[1*]

[1] European Synchrotron Radiation Facility (ESRF) 6 Rue Jules Horowitz, BP 220 38043 Grenoble Cedex 9 France
[2] Department of Inorganic, Physical and Materials Chemistry, INSTM Reference Center and NIS Centre of Excellence, Università di Torino, Via P. Giuria 7, I-10125 Torino, Italy.
[3] Sciences Chimiques de Rennes - UMR 6226, Matériaux Inorganiques: Chimie Douce et réactivité, Université de Rennes 1, Campus de Beaulieu, Bât 10B, F-35042 Rennes, France.

In Figure SI, the spectra computed using TZVP/CP(PPP) basis sets and TPSSh density functional on the cluster T35_MFI are reported, changing the Ti position in the framework. As clearly visible from the figure no T-dependency was found. This is due to the local character of the technique.

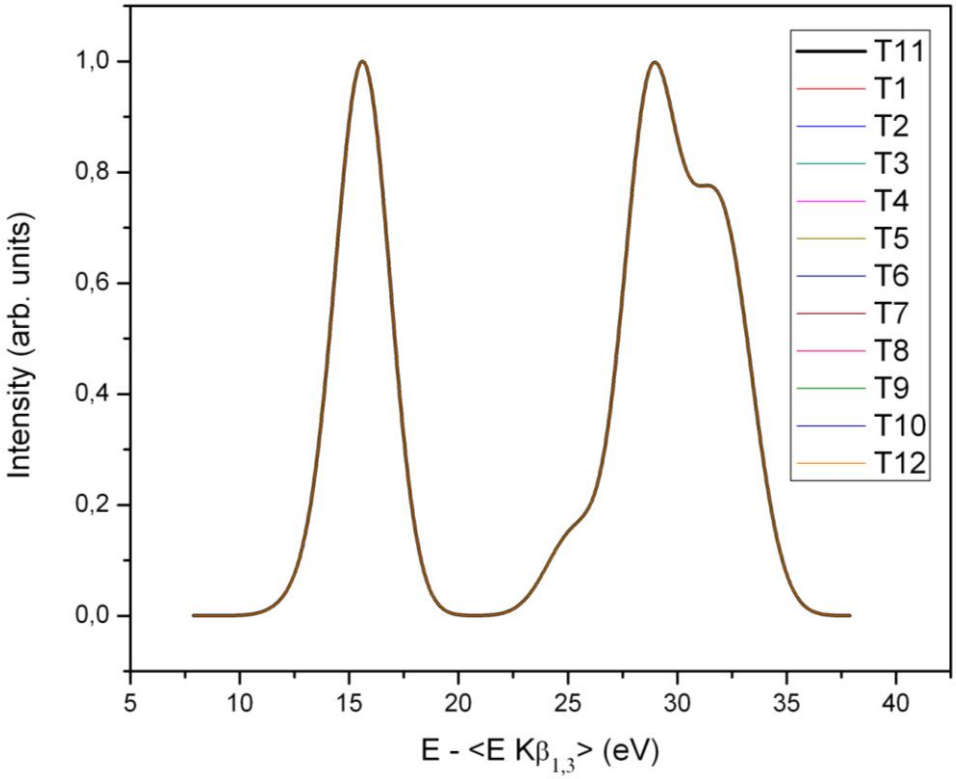

Figure S1: VtC-XES spectra computed adopting TPSSh/TZVP/CP(PPP) on the clusters T35_MFI**,** optimized with the Ti atom in one of the twelve non equivalent crystallographic positions.

[2] Corresponding authors: carlo.lamberti@unito.it, pieter.glatzel@esrf.

Table 3. Goodness factors for the VtC-XES spectra computed on the T5OH cluster using TZVP(ligands)/CP(PPP)(Ti) for a selection of density functionals.

Functional	ΔE_{max} (eV)	ΔE_{cm} (eV)	I_C/I_B ratio (±0.005)
LDA	17.7	17.9	0.829
GLYP	12.4	12.66	0.738
PBE	12.5	13.03	0.779
PWP	12.6	12.7	0.802
B1LYP	13.7	14.5	0.744
B3LYP	13.4	13.6	0.773
PBE0	13.8	14.1	0.79
TPSS	13.0	13.6	0.821
TPSSh	13.2	13.8	0.780
TPSS0	14.3	15.0	0.840
B2PLYP	15.2	16.1	0.823
Experiment	13.2	13.8	0.781